ENGINEERING SCIENCES

Characterization and application of magnetic biochar for the removal of phosphorus from water

TERESA CRISTINA F. SILVA, LEONARDUS VERGÜTZ, ANDERSON A. PACHECO, LARISSA F. MELO, NATALIA S. RENATO & LEÔNIDAS C.A. MELO

Abstract: Activated biochars were prepared from residues of medium density fiberboard (MDF) produced by the furniture industry. Biomass residue was pre-treated with $FeCl_3$ in two different $FeCl_3$:biomass ratios (0.5:1 and 1:1, w/w) aiming to produce a matrix embedded with iron oxide. The pyrolysis process produced maghemite on the biochar surface and its magnetic properties were confirmed by its attraction to a hand magnet and its magnetic susceptibility. Samples were also characterized using scanning electron microscopy with energy dispersive spectroscopy (SEM/EDS), surface area by BET-N_2, Fourier transform infrared (FTIR), X-ray diffraction, magnetic susceptibility, and cation exchange capacity (CEC). Magnetic biochar exhibited up to twelve-fold higher surface area than the non-magnetic biochar, which varies according the maghemite particles content. Iron oxide on biochar surface also contributed for increasing CEC around ten-fold compared to non-magnetic biochars. Phosphorus adsorption isotherms showed that these magnetic biochars have high capacity to sorb oxyanions like phosphate, especially at lower pH. Thus, these magnetic biochars could be used to clean water bodies contaminated with oxyanions in acidic conditions.

Key words: adsorption, biochar, eutrophication, isotherms, phosphorus, water treatment.

INTRODUCTION

Phosphorus (P) is a limiting nutrient that keeps plants and algae from growing in water bodies, being a limiting factor for eutrophication. The excess of P-containing fertilizers that are leached through the soil or carried as runoff is a major cause of water bodies eutrophication, together with residues from mineral deposits and anthropogenic sources such as municipal domestic and industrial wastewater (Xiang et al. 2014). A concentration as low as 0.02 mg/L of phosphate would lead to uncontrolled growth of algae, resulting in oxygen depletion and production of toxins in water bodies, leading to fish death and degrading water quality for human and animal consumption (Li et al. 2016).

The most practical and highly adopted way of removing P from water bodies is through its sorption on a sorbent material (Xiang et al. 2014). Removal of phosphate from water has been reported using inorganic sorbents such as metal oxides and hydroxides, calcium and magnesium carbonates and hydroxides and layered double hydroxides (Chitrakar et al. 2006, Goh et al. 2008, Khadhraoui et al. 2002, Makris et al. 2005, Zhou & Haynes 2010), whereas organic sorbents include activated carbon and anion exchange resins (Blaney et al. 2007, Gupta et al. 2012, Shi et al. 2011). Among the sorbents, biochar has been receiving increasing attention over the years because it is relatively easy and cheap to prepare (Jeong et al. 2016). As a result,

research has focused on the application of biochar for cleaning contaminated waters and for the phosphate recovery and reuse. However, biochar negatively charged surfaces has limited its ability and applications to sorb and clean anionic pollutants (Chen et al. 2011, Li et al. 2016).

Biochars are high-carbon stable solid residues produced through the pyrolysis process of biomass – heating in absence of oxygen. Its unique properties such as high surface area, cation exchange capacity, and abundant functional groups favors its use as adsorbent to remove pollutants from aqueous solutions. An enormous variety of feedstock has been used to produce biochar as well as many chemical modifications techniques that improve biochar functioning in wastewater treatment applications (Tan et al. 2015). Magnetic biochar has been successfully produced among these approaches by precipitation of iron oxides onto the surfaces of biochars. A great advantage of magnetic biochar use is that its separation simplifies isolation and washing followed by redispersion.

The application of magnetic biochar to solve environmental problems has gained considerable attention recently due to their efficiency to adsorb compounds dissolved in aqueous solutions (Chen et al. 2011, Zhang et al. 2013). Magnetic biochar applications in anion removal have been reported to fluoride (Mohan et al. 2014, Oh et al. 2012), nitrate (Zhang et al. 2012) and phosphate (Chen et al. 2011, Zhang et al. 2012, 2013). The removal of phosphate from aqueous solutions using magnetic biochar has another great benefit as the it can be used afterward as a slow release P fertilizer in the soil (Yao et al. 2011, 2013), increasing plants P recovery.

The aim of the present work was to give destination to a common residue of the furniture industry that is the sawdust powder of medium density fiberboard (MDF). The objective was to prepare different biochars with this residue and evaluate its capacity to sorb phosphate from contaminated water bodies. The biochars produced here were characterized by infrared spectroscopy, surface area, X-ray diffraction, magnetic susceptibility, scanning electron microscopy, and P adsorption capacity from pHs 1 to 4.

MATERIALS AND METHODS

Biochar production

The magnetic biochar was synthesized from medium density fiberboard (MDF) powder residue. MDF powder was immersed for 2 h in a saturated ferric chloride solution in two different weight proportions of MDF:$FeCl_3$ – 1:1 and 1:0,5 (w/w). Under stirring, 5 mol/L NaOH solution was added to raise suspension pH to 10-11. Subsequently, the solid fraction was decanted and then dried at 80 ^{o}C for 24 h in a forced air furnace. For comparison, a blank sample was produced in the same way, without the addition of $FeCl_3$. Each sample of pre-treated biomass filled three pots of 1 litter with no space left and covered with a lid for pyrolyzing in a furnace at a temperature of 400 ^{o}C in absence of O_2 for one hour at the heating rate of 10 ^{o}C/min. After cooling down, the pot was taken out and the biochar was manually crushed. The biochars were then washed several times with deionized water (DI), oven-dried at 80 ^{o}C until constant weight and sealed in three containers referred to as CBC (control biochar), 0,5 FeBC and 1,0 FeBC, where the prefix numbers represent the $FeCl_3$ weight ratio related to MDF.

Biochar characterization

Cation exchange capacity (CEC) of the biochar was measured using ammonium-acetate displacement, following the method described

by Blaney et al. (2007). Samples were firstly washed five times with DI water to minimize interference of soluble salts. A flame photometer was used to measure sodium ions displaced with ammonium acetate.

Fourier transform infrared (FTIR) spectra were performed using a VARIAN 660-IR instrument with attenuated total reflectance PIKE GladiATR sampling accessory. For each sample, 256 scans in the 4000-400 cm⁻¹ spectral range were collected.

Specific surface areas were obtained from N_2 adsorption-desorption isotherms measured at 77 K on a NOVA 1200 Quantachrome analyzer and calculated using Brunauer-Emmett-Teller (BET) method. All samples were outgassed at 150 °C prior to analysis for a minimum of 6 h. BET surface areas were taken from a multipoint plot over a P/Po range of 0.05-0.1.

Surface elemental composition and surface distribution maps were obtained with scanning electron microscope (SEM) using a Leo 1430 VP coupled with energy dispersive X-ray spectroscopy (EDS, LXRF Model 550).

X-ray diffraction (XRD) analyses were carried out on randomly oriented biochars powder to identify crystallographic structures, using a Shimadzu XRD 6000 diffractometer (CuKα radiation). X-ray diffraction (XRD) patterns were collected between 4 and 70 °2θ, and a scan speed of 1 °2θ min⁻¹, with an acceleration of 30 kV and 30 mA of current.

Magnetic properties of the biochars were measured at room temperature using a Bartington® MS2 Magnetic Susceptibility System, with the MS2B sensor. The volumetric magnetic susceptibility (k) was measured at low (0,465 kHz – $k$lf) and high (4,65 kHz – $k$hf) frequencies ± 1 %. The low-frequency mass magnetic susceptibility (χlf) was calculated as follows (Dearing 1999), considering the equation:

$$[\chi\text{lf}=(10 \, x \, k\text{lf})/m] \hspace{2cm} \text{Eq. 1}$$

where m is the mass (g).

Phosphorus sorption isotherms

Sorption isotherms for CBC, 0,5FeBC and 1,0FeBC consisted of 10 phosphate concentration points and were carried out at pHs 1, 2, 3 and 4. Each isotherm was carried out in duplicate. In order to achieve the desired pH for each biochar, a known mass of sample was suspended in a minimum amount of water and magnetically stirred while solutions of HCl or KOH were added dropwise until pH was reached. Then, the flasks were placed on a rotating shaker for 24 h until equilibrium. Samples were dried under air and 0.1 g of biochar samples were placed in 50 mL centrifuge tubes and suspended in 25 mL of 0.01 mol L⁻¹ KCl solution containing 0, 1, 2, 3, 5, 8, 11, 14, 17, and 20 mg L⁻¹ of P added as KH_2PO_4. At the end of the equilibration period (24 hours), the samples were decanted for 2 hours and the supernatant was filtered through a 0.45 μm membrane filter.

Phosphate was quantified by molecular absorption spectrophotometry (colorimetry) method at a wavelength of 725 nm, after reaction with ascorbic acid and ammonium molybdate (Braga & Defelipo 1974). The sorbed P was quantified as the difference between the initial amount of P added and the amount in the equilibrium solution. All the sorption data are presented as arithmetic means of the duplicates in the present study.

The P sorption data obtained have been analyzed using four models (linear, Freundlich, Langmuir and Langmuir-Freundlich) to predict the adsorption isotherms and to determine its characteristic parameters. The equations related to the models studied are as follows:

Linear model: $q_e = kc_e + m$ \hspace{1.5cm} (Eq. 2)

Langmuir model: $q_e = \dfrac{kQc_e}{1+kc_e}$ (Eq. 3)

Freundlich model: $q_e = k_f c_e^n$ (Eq. 4)

Langmuir-Freundlich: $q_e = \dfrac{kQc_e^n}{1+kc_e^n}$ (Eq. 5)

where q_e is the amount of P sorbed at the equilibrium (mg g^{-1}); K and K_f represent, respectively, the Langmuir constant (L mg^{-1}) and Freundlich capacity coefficient (mg g^{-1})/ (mg L)^n); c_e is the equilibrium solution concentration (mg L^{-1}) of the adsorbate and n is the Freundlich linearity constant.

In order to choose the two models that exhibited the better suitability with the experimental data, we based on the standard error of regression (SE) and adjusted R-square (R^2_{Adj}). The final model was chosen by comparing Akaike information criterion (AIC) with Bayesian information criterion (BIC) methods. All data manipulation was performed using the Origin® software.

RESULTS AND DISCUSSION

Biochars characterization

Magnetic biochar was successfully produced by the pyrolysis. It was confirmed by the readily attraction of 0.5FeBC and 1.0FeBC samples by a magnet, even after thoroughly washing the biochars; facilitating magnetic separation technique in aqueous solution and laying emphasis on magnetic biochar potential for further use. It has been reported (Mohan et al. 2014) that biochar surfaces help nucleate iron oxide precipitation, in alkaline media, through a tightly chemical bond between oxygenated groups (hydroxyl and carboxyl) presented in the biochar and iron hydroxide/oxide in solution, producing the mineral onto the biochar.

The Fourier transform infrared spectroscopy (FTIR) was done to evaluate the formation of functional groups that could act as an active center for adsorption. The FTIR spectra of non-magnetic (CBC) and magnetic biochars (0.5FeBC and 1.0FeBC) are shown in Figure 1. Both magnetic biochars (0.5FeBC and 1.0FeBC) revealed similar spectra. The spectra exhibits the presence of functional groups containing oxygen atoms that could act as hubs for chemical sorption, enhancing the adsorption capacity of the adsorbent (Lu et al. 2008).

The broad band at 3345 cm^{-1} (Figure 1) are attributed to O-H stretch from carboxylic groups (-COOH and -COH) (Chen et al. 2011, El-Hendawy 2006). The signals observed at 2962, 2919, 2887 cm^{-1} were attributed to C–H stretching from aromatic compounds (El-Hendawy 2006, Wang et al. 2004, Zhong et al. 2002). The peaks 2659, 2362, and 2333 cm^{-1} can be related to O-H stretch from strong H-bonded-COOH from carboxylic groups (Davis et al. 1999, Gao et al. 2009, Lu et al. 2008). The region of 1600 – 1000 cm^{-1} is very complex because of the contribution of many different functional groups in the MDF residue and also inorganic material present in the original material. A broad absorbance peak at 1560 and 1436 cm^{-1} is ascribed as C=C stretching vibrations due to aromatic and carboxylic compounds, and C=O for a stretching vibrations from carboxylic compounds, created by cyclization reactions under high temperatures (El-Hendawy 2006, Wang et al. 2004, Zhong et al. 2002). At 1375 and 1313 cm^{-1} is due to C=C stretching vibrations from aromatic compounds and C-O + O-H vibrations referring to the combination of the C-O stretch and the angular deformation of O-H from carboxylic groups (Chen et al. 2011). The signals observed at 1268, 1186, 1033 cm^{-1} were attributed to C–H stretching vibrations from aromatic compounds with angular deformation in the plane and stretching of the carboxylic
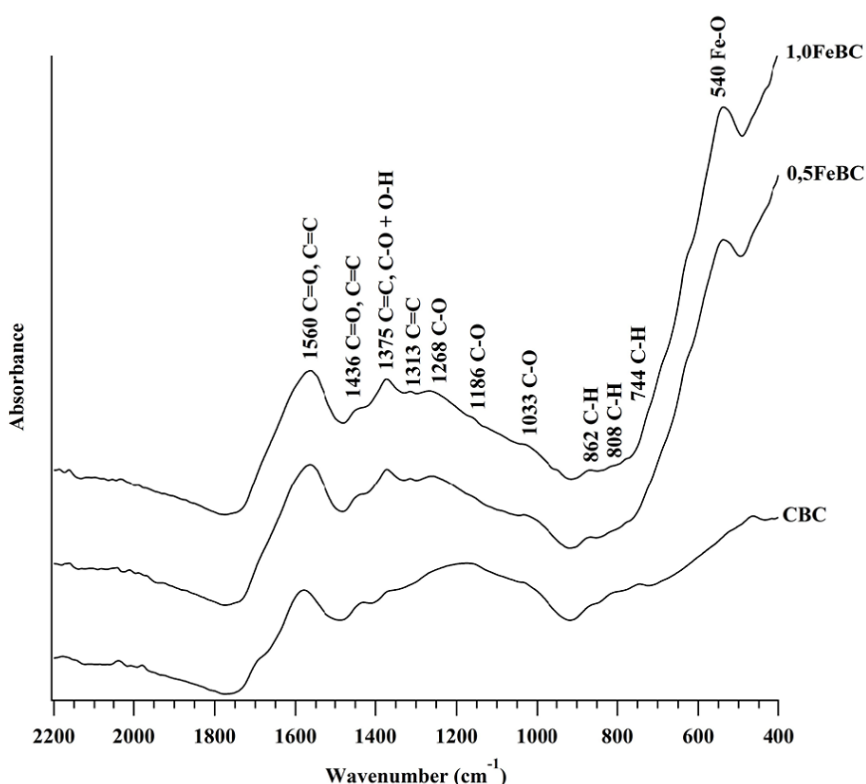
Figure 1. Fourier transform infrared spectra of three biochar samples. (a) range 4000 to 2200 cm^{-1}, and (b) range 2200 to 400 cm^{-1}.

compounds (Raj et al. 2009). The C-H vibrations at 862, 808, 744 cm^{-1} can be related to aromatic compounds with angular deformation outside the plane, caused by the pyrolysis of the biochar, since it appears only in the CBC (Denyes et al. 2014). The strong broad peak at approximate 540 cm^{-1} is assigned to Fe–O of iron oxides (Lim et al. 2009, Santos et al. 2016). The broad peak at approximately 540 cm^{-1} for all magnetic biochars (0.5FeBC and 1.0FeBC) confirm the production of iron oxides onto the magnetic biochars (Chen et al. 2011).

The X-ray diffraction (XRD) pattern (Figure 2) obtained from the control biochar (CBC) showed the presence of cellulose, confirmed by their interplanar *d* spacing at 0.589 and 0.379 nm, indicating an incomplete cellulose degradation at 400 °C (Kloss et al. 2012). The magnetic biochars (1.0FeBC and 0.5FeBC) showed XRD pattern (Figure 2) of well crystallized minerals, proved to be composed exclusively of maghemite

(γ-Fe$_2$O$_3$), with interplanar *d* spacing of 0.295, 0.252, 0.208, 0.169, 0.161 and 0.148 nm (Cornell & Schwertmann 2003). These features confirmed the success in the synthesis of the biochar/γ-Fe$_2$O$_3$ composite under study (Campos et al. 2015, Chen et al. 2011, Machala et al. 2011). The 1.0FeBC biochar/γ-Fe$_2$O$_3$ composite was synthetized with double of the FeCl$_3$ than 0.5FeBC as previously reported. Evaluating the relative intensities of the XRD (Figure 2) the 1.0FeBC showed higher intensity peaks than 0.5FeBC, indicating an increase on maghemite with higher FeCl$_3$ weight ratio related to MDF.

The magnetic susceptibility indicates the magnetic behavior of the biochars (Table I). As expected, the control biochar (CBC) has no magnetic properties and is characterized as a diamagnetic material (Dearing 1999). The other biochars, produced with FeCl$_3$, showed great ferromagnetic properties, being characterized as a ferrimagnetic material by presenting a strong
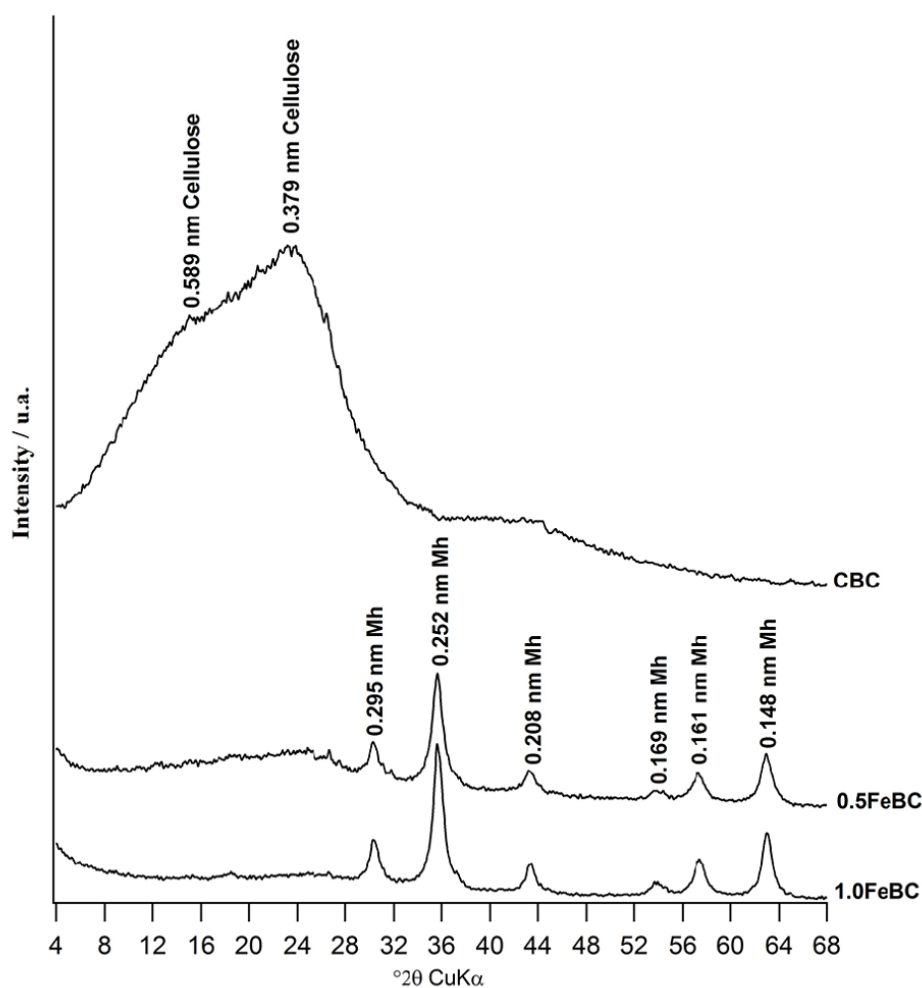
Figure 2. X-ray diffraction (XRD) pattern collected from biochar (CBC) and biochar/γ-Fe$_2$O$_3$ composite (0.5FeBC and 1.0FeBC). Mh – Maghemite.

positive susceptibility (Teja & Koh 2009). The low-frequency magnetic susceptibility (χlf) was 12701.04 10^{-8} m^3 Kg^{-1} for the 0.5FeBC and 19557.18 10^{-8} m^3 Kg^{-1} for the1.0FeBC, with iron contents of 29.25 and 43.30 %, respectively. These results corroborated with Dearing (1999), which reported χlf values for pure maghemite (γ-Fe$_2$O$_3$) ranging from 28600 to 44000 10^{-8} m^3 Kg^{-1} and magnetite from 39000 to 111600 10^{-8} m^3 Kg^{-1} with up to 72 % of iron. Different features like the mineral concentration and composition, crystal size and domains, and crystal shape can explain the lower χlf of the 0.5FeBC than the 1.0FeBC biochar (Dearing 1999). According to other studies, it probably happened due to the lower Fe content and the presence of diamagnetic elements (C, Na and P) at the composite biochar, which reduced the magnetic moment of the mineral (Barrn & Torrent 2002, Dearing et al. 1996).

The dual frequency magnetic susceptibility (χfd%) varied from 5.90 to 6.17 % (Table I), which according (Dearing 1999) could be a mixture of superparamagnetic (SP) and coarser non-SP grains or SP grains <0.005 µm. This behavior come up with very small particle size of the biochar/γ-Fe$_2$O$_3$ composite produced according χfd% values (Dearing 1999). Thus, the positive correlation of the χfd% with the specific surface area and Fe content , demonstrates the strong dependence of magnetization on particle size (Heider et al. 1996, Maher 1988).

SEM images show surface morphology of the three studied biochars (Figure 3). It can be seen that both magnetic biochars (0.5FeBC and 1.0FeBC) have good dispersion of γ-Fe_2O_3 particles, suggesting that pyrolysis soldered and stabilized the maghemite particles on biochar surface (Zhang et al. 2013, Zhang & Gao 2013). In fact, during pyrolysis, the char surfaces acts as a base for nucleation and precipitation of iron oxide particles. Thus, γ-Fe_2O_3 particles are partly embedded in the biochar matrix, indicating good mechanical bonding and consequently preventing separation of the γ-Fe_2O_3 particles from the biochar matrix. The result from EDS spectra of 0.5FeBC and 1.0FeBC biochars comprises mainly three elements: oxygen, carbon and iron (Table II). It is worth mention that, even though the amount of Fe^{3+} added in 1.0FeBC was two times higher, the EDS revealed 40 % weight of Fe against 30 % for 0.5FeBC sample.

Surface area of the biochars exhibit considerably differences, even for the magnetic samples (Table III). The presence of γ-Fe_2O_3 particles in the biochar increases the surface area up to twelve-fold compared to non-magnetic biochar (CBC), and 1.0FeBC had surface area higher than 0.5FeBC. These results show that the content of ferromagnetic material in the biochar increased its specific surface area, in agreement with previous work (Han et al. 2016, Park et al. 2008) increasing its adsorption capacity (Ahmad et al. 2012).

Cation exchange capacity (CEC) of the biochars, in all pH studied, are given in Table III. Non-magnetic biochar (CBC) presented, on average, 10 times lower CEC (from 34.6 to 37.4 $cmol_c$ kg^{-1}) compared to the magnetic biochars. Part of this CEC increase is due to higher surface area of the Fe-treated biochars. Surface area of the biochars (Table III) and SEM images (Figure 3) lead to assert that the presence of Fe^{3+} during

Table I. Magnetic susceptibility from biochar and biochar/γ-Fe_2O_3 composite.

Sample	κ_{lf}	κ_{hf}	X_{lf}	X_{fd}
	10^{-8} m^3 kg^{-1}			%
CBC	0.00	0.00	0.00	0.00
0.5FeBC	3372	3164	12701.04	6.17
1.0FeBC	7137	6716	19557.18	5.90

Table II. EDS spectra result.

Element	Line	Concentration		
		Wt. %		
		CBC	0.5FeBC	1.0FeBC
C	Kα	-	41.884	33.912
O	Kα	81.742	23.949	21.792
Na	Kα	11.485	4.811	4.817
P	Kα	4.599	0.107	0.175
Fe	Kα	2.173	29.25	39.303

the pyrolysis helps to break down the C structure into smaller particles. However, this increase on CEC is not just due to the greater surface area; once CEC on the 0.5FeBC was higher, presenting surface area three-fold lower than 1.0FeBC. The 0.5FeBC presented CEC ranging from 374 to 417 $cmol_c$ kg^{-1}, while CEC of 1.0FeBC ranged from 278 to 347 $cmol_c$ kg^{-1}. The increased CEC of the magnetic biochar with less ferromagnetic material (0.5FeBC) is associated with the presence of more adsorption sites available to form oxygenated functional groups (hydroxyl, carbonyl and carboxylate), thus enhancing the negative charge density at the surface of that biochar. FTIR spectra (Figure 1) of magnetic biochars showed more functional groups on its surface than non-magnetic biochar, which brings more negative charges and increases CEC. However, there are no great differences between the magnetic biochars in terms of functional groups (Figure 1). Basically, the 1.0FeBC, treated with higher amount of Fe^{3+}, showed higher
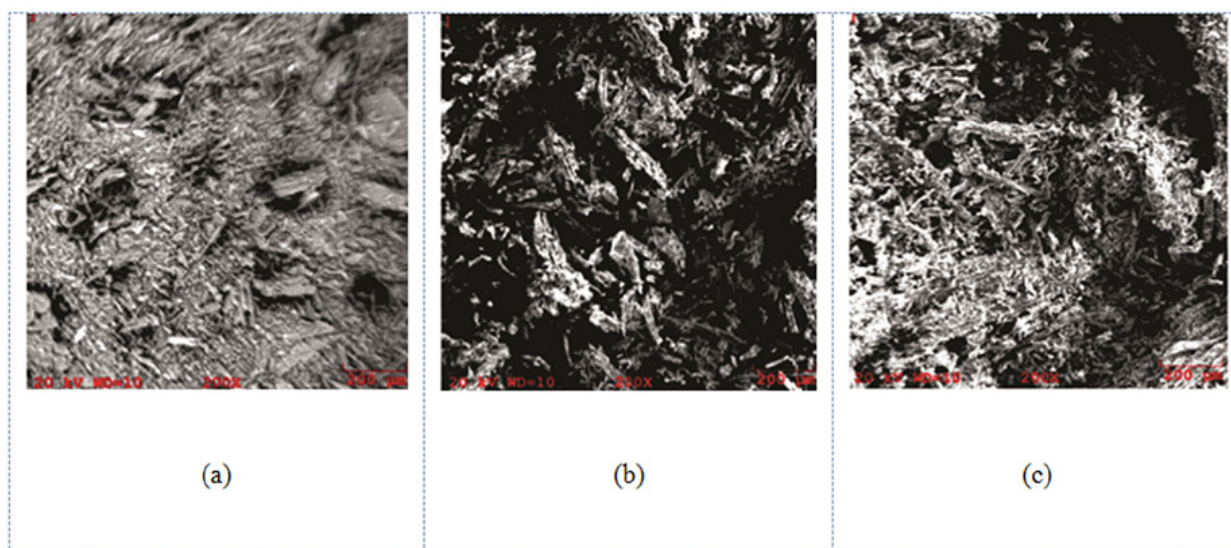
Figure 3. SEM-EDS image of (a) CBC, (b) 0.5FeBC, and (c) 1.0FeBC.

Table III. Surface area and Cation Exchange Capacity (CEC) of biochars.

CBC			0.5FeBC			1.0FeBC		
Surface area $(m^2 g^{-1})$	pH	CEC $cmol_c kg^{-1}$	Surface area $(m^2 g^{-1})$	pH	CEC $cmol_c kg^{-1}$	Surface area $(m^2 g^{-1})$	pH	CEC $cmol_c kg^{-1}$
2.309	1.0	37.4	9.338	1.0	382.6	28.758	1.0	347.8
	2.0	34.8		2.0	373.9		2.0	278.3
	3.0	36.0		3.0	374.2		3.0	295.6
	4.0	34.6		4.0	417.4		4.0	339.1

intensity on the Fe-O peak. On the other hand, the 0.5FeBC showed an increase on the intensity of the 2362-2333 cm^{-1} peak, related to the O-H. The increase of these functional groups on the surface of the biochar is probably the main reason for the higher CEC of 0.5FeBC.

Phosphate sorption

Four isotherm models (linear, Langmuir, Freundlich and Langmuir-Freundlich) were used to fit adsorption isotherms of phosphate to the CBC, 0.5FeBC and 1.0FeBC biochars at pHs ranging from 1 – 4, to determine which isotherm gives the best correlation to the experimental data. Table IV shows standard error (SE) and adjusted determination coefficients (R^2_{adj}) of isotherms data. In general, both Freundlich and Langmuir-Freundlich models fitted well with lower SE and higher R^2_{adj}. For this reason a matched-pair comparison was performed. Based on AIC and BIC, it was observed that Freundlich isotherm best fits the equilibrium data for phosphate adsorption in 11 out of 12 isotherms. Freundlich theory indicates multilayer adsorption of $H_2PO_4^-$ over the heterogeneous surface, with non-uniform distribution of adsorption (Foo & Hameed 2010). According to this model, the amount adsorbed is the sum of adsorption on all sites, with the stronger binding sites occupied first, until adsorption energy are exponentially

Table IV. Standard error (SE) and determination coefficients (R^2) of isotherms data in linear, Freundlich, Langmuir and Langmuir-Freundlich models.

	pH	Linear		Freundlich		Langmuir		Langmuir-Freundlich	
		SE	R^2_{Adj}	SE	R^2_{Adj}	SE	R^2_{Adj}	SE	R^2_{Adj}
CBC	1	0.010	0.973	0.016	0.923	0.042	0.500	0.006	0.991
CBC	2	0.017	0.985	0.017	0.985	0.028	0.959	0.019	0.983
CBC	3	0.024	0.976	0.297	-2.598	0.028	0.967	0.027	0.970
CBC	4	0.030	0.953	0.029	0.958	0.033	0.946	0.031	0.950
0.5FeBC	1	0.282	0.883	0.185	0.950	0.125	0.977	0.127	0.976
0.5FeBC	2	0.152	0.952	0.100	0.979	0.264	0.856	0.110	0.975
0.5FeBC	3	0.265	0.871	0.054	0.995	0.131	0.968	0.029	0.998
0.5FeBC	4	0.101	0.928	0.046	0.985	0.136	0.868	0.050	0.983
1.0FeBC	1	0.154	0.931	0.035	0.996	0.124	0.955	0.038	0.996
1.0FeBC	2	0.178	0.932	0.070	0.989	0.194	0.919	0.076	0.988
1.0FeBC	3	0.234	0.894	0.083	0.987	0.123	0.971	0.073	0.990
1.0FeBC	4	0.092	0.918	0.047	0.979	0.106	0.891	0.051	0.975

decreased upon the completion of adsorption process (Sun et al. 2015).

Table V shows the coefficients obtained for Freundlich model. P isotherms of adsorption based-Freundlich model are shown on Figure 4. In general, the presence of magnetic mineral in the biochar (0.5FeBC and 1.0FeBC) increased by more than five-fold the adsorption of phosphate. The maximization of adsorption capacity in magnetic samples was attributed to the increased surface area and also to the generation of positive charges by the iron oxide (Sun et al. 2015). Also, iron oxides are known for their high P adsorption capacity and for adsorbing P specifically, with great energy.

In general, CBC showed the worst P adsorption capacity (Fig. 4), while the magnetic biochars showed higher adsorption capacities. CBC performed better at pHs 2.0, 3.0 and 4.0, whereas at pH 1.0 it showed the worst performance (Figure 4A). Points of zero charge (PZC) of biochars are generally low (Essandoh et al. 2015, Liu et al. 2012, Zheng et al. 2013). In this sense, decreasing solution pH increases

positive charges on the biochar surface, even though not as much as in high PZC materials. Thus, P adsorption onto CBC should be higher the lower the pH. However, the decrease of P adsorption at pH 1 can be explained by the change on P speciation. At pH 1, almost 100 % of all phosphate in solution is in the form of the neutral H_3PO_4. As biochars (and other organic materials) do not adsorb P specifically (chemisorption) and electrostatic attraction is the driving force of this interaction, the lack of charge on the sorbate (H_3PO_4) decreases total adsorption capacity.

On the other hand, 0.5FeBC and 1.0FeBC showed higher phosphate adsorption at low pH (1.0, 2.0 and 3.0) and higher affinity (Figures 4b and 4c). Maghemite formed onto the biochars surface showed an average PZC of 5.9, but other Fe_2O_3 oxides (also probably formed) can show PZC as high as 9 (Benjamin et al. 1996, Kosmulski 2001). Thus, lower pH increases the amount of positive charges on the surface of these minerals, increasing electrostatic attraction of anions like phosphate and its adsorption capacity. As pH
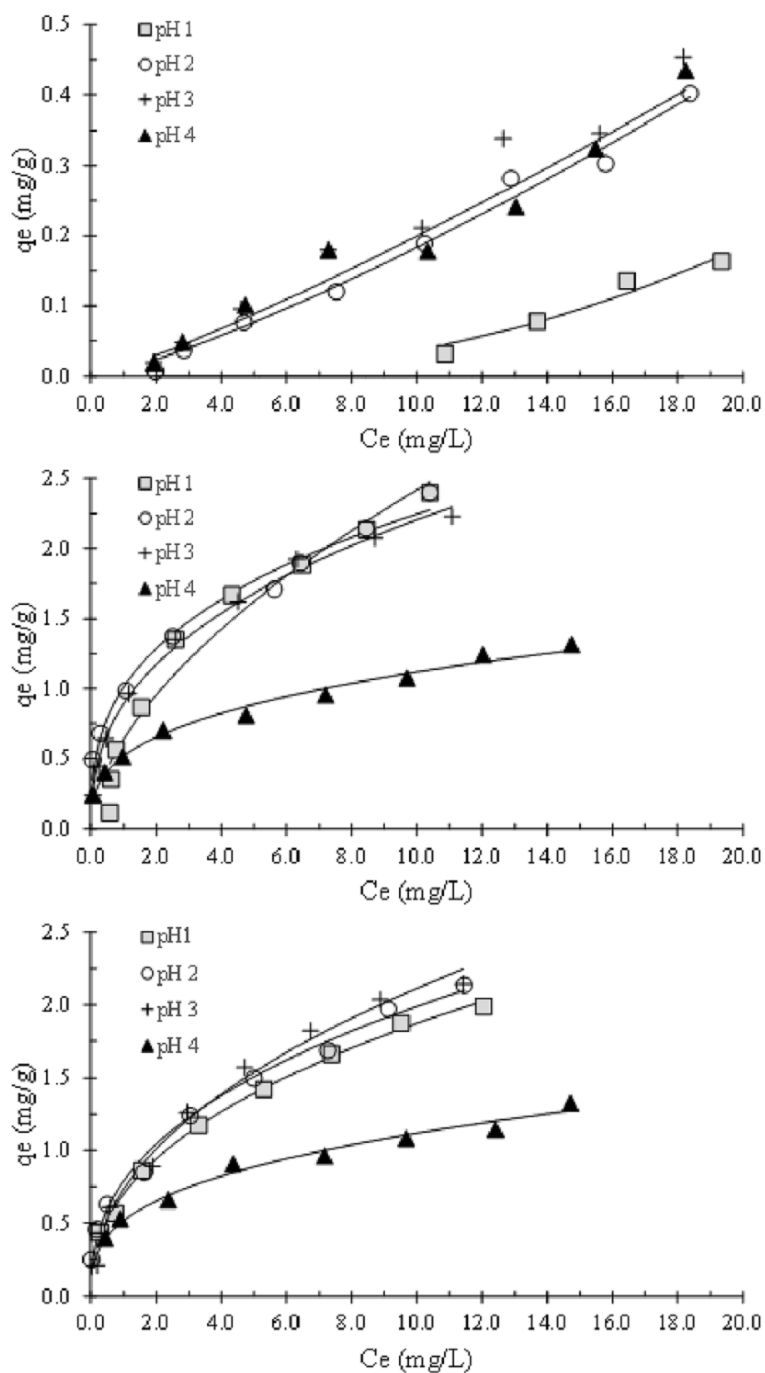
Figure 4. Adsorption isotherms adjusted by Freundlich model for (a) CBC, (b) 0.5FeBC and (c) 1.0FeBC sample in pH 1 to 4.

Table V. Parameters for Freundlich model.

	CBC pH 1	CBC pH 2	CBC pH 3	CBC pH 4	0.5FeBC pH 1	0.5FeBC pH 2	0.5FeBC pH 3	0.5FeBC pH 4	1.0FeBC pH 1	1.0FeBC pH 2	1.0FeBC pH 3	1.0FeBC pH 4
Kf	0.00017	0.64198	0.70371	0.00995	1.01493	0.03508	3.4E-16	0.89565	0.73767	0.01311	0.51763	0.52438
n	0.42881	1.73612	2.35539	0.79003	2.90061	0.14043	0.82117	2.55736	2.18957	0.84572	2.98759	3.06315

raises, sorbent surface becomes more negatively charged and repulsion takes place, especially at pH 4, when also P species in solution are 100 % $H_2PO_4^-$. But despite the adsorption decrease at pH 4, P is chemisorbed on iron oxides and pH 4 is still lower than the PZC of these oxides, keeping the surface of these minerals positively charged on the biochars.

Between the Fe activated biochars, 0.5FeBC adsorbs slightly more P (2.4 mg/g) than the 1.0FeBC (2.2 mg/g), which is a very good adsorption capacity in comparison to other biochars (Chen et al. 2011). Assuming that arsenate dynamics is similar to phosphate, these biochars show an interesting capacity to sorb arsenate to clean contaminated waters (Zhang et al. 2013, Zhang & Gao 2013), specially in low pH conditions like Acid Mine Drainage.

CONCLUSIONS

Medium density fiberboard (MDF) residue proved to be an excellent material for the production of biochar at low cost. From this biochar was possible to synthesize two magnetic biochar/ γ-Fe2O3 composite (0.5FeBC and 1.0FeBC) with great P adsorption capacity due to the formation of maghemite on its surface.

The magnetic biochar/γ-Fe2O3 composite (0.5FeBC and 1.0FeBC) showed higher adsorption capacity of P in solution than non-magnetic biochar (CBC), with 0.5FeBC presenting slightly better results. Therefore, the characteristics presented by synthesized magnetic biochars represent an alternative to remediate water bodies with pollutants like phosphorus (the main cause of eutrophication) and elements exhibiting similar chemical characteristics.

REFERENCES

AHMAD M, LEE SS, DOU X, MOHAN D, SUNG JK, YANG JE & OK YS. 2012. Effects of pyrolysis temperature on soybean stover- and peanut shell-derived biochar properties and TCE adsorption in water. Bioresour Technol 118: 536-544.

BARRN V & TORRENT J. 2002. Evidence for a simple pathway to maghemite in Earth and Mars soils. Geochim Cosmochim Acta 66: 2801-2806.

BENJAMIN MM, SLETTEN RS, BAILEY RP & BENNETT T. 1996. Sorption and filtration of metals using iron-oxide- coated sand. Water Res 30: 2609-2620.

BLANEY L, CINAR S & SENGUPTA A. 2007. Hybrid anion exchanger for trace phosphate removal from water and wastewater. Water Res 41: 1603-1613.

BRAGA JM & DEFELIPO BV. 1974. Determinação espectrofotométrica de fósforo em extratos de solo e material vegetal. Ceres 21: 73-85.

CAMPOS EA, STOCKLER PINTO DVB, OLIVEIRA JIS, MATTOS EC & DUTRA RCL. 2015. Synthesis, characterization and applications of iron oxide nanoparticles - a short review. J Aerosp Technol Manag 7: 267-276.

CHEN B, CHEN Z & LV S. 2011. A novel magnetic biochar efficiently sorbs organic pollutants and phosphate. Bioresour Technol 102: 716-723.

CHITRAKAR R, TEZUKA S, SONODA A, SAKANE K, OOI K & HIROTSU T. 2006. Phosphate adsorption on synthetic goethite and akaganeite. J Colloid Interface Sci 298: 602-608.

CORNELL RM & SCHWERTMANN U. 2003. The iron oxide – structure, properties, reactions, occurrences and use. Wiley – VCH Verlag GmbH & Co.KGaA, Weinheim.

DAVIS WM, ERICKSON CL, JOHNSTON CT, DELFINO JJ & PORTER JE. 1999. Quantitative Fourier Transform Infrared spectroscopic investigation humic substance functional group composition. Chemosphere 38: 2913-2928.

DEARING JA. 1999. Environmental Magnetic Susceptibility. Using the Bartington MS2 system, 2nd ed., Chi Publications, Kenilworth, UK.

DEARING JA, DANN RJL, HAY K, LEES JA, LOVELAND PJ, MAHER BA & O'GRADY K. 1996. Frequency-dependent susceptibility measurements of environmental materials. Geophys J Int 124: 228-240.

DENYES M, PARISIEN MA, RUTTER A & ZEEB BA. 2014. Physical, chemical and biological characterization of six biochars produced for the remediation of contaminated sites. J Vis Exp e52183.

EL-HENDAWY ANA. 2006. Variation in the FTIR spectra of a biomass under impregnation, carbonization and oxidation conditions. J Anal Appl Pyrolysis 75: 159-166.

ESSANDOH M, KUNWAR B, PITTMAN CU, MOHAN D & MLSNA T. 2015. Sorptive removal of salicylic acid and ibuprofen from aqueous solutions using pine wood fast pyrolysis biochar. Chem Eng J 265: 219-227.

FOO KY & HAMEED BH. 2010. Insights into the modeling of adsorption isotherm systems. Chem Eng J 156: 2-10.

GAO Z, BANDOSZ TJ, ZHAO Z, HAN M & QIU J. 2009. Investigation of factors affecting adsorption of transition metals on oxidized carbon nanotubes. J Hazard Mater 167: 357-365.

GOH KHH, LIM TTT & DONG Z. 2008. Application of layered double hydroxides for removal of oxyanions: A review. Water Res 42: 1343-1368.

GUPTA M, LOGANATHAN P & VIGNESWARAN S. 2012. Adsorptive removal of nitrate and phosphate from water by a purolite ion exchange resin and hydrous ferric oxide columns in series. Sep Sci Technol 47: 1785-1792.

HAN Y, CAO X, OUYANG X, SOHI SP & CHEN J. 2016. Adsorption kinetics of magnetic biochar derived from peanut hull on removal of Cr (VI) from aqueous solution: Effects of production conditions and particle size. Chemosphere 145: 336-341.

HEIDER F, ZITZELSBERGER A & FABIAN K. 1996. Magnetic susceptibility and remanent coercive force in grown magnetite crystals from 0.1 μm to 6 mm. Phys Earth Planet Inter 93: 239-256.

JEONG CY, DODLA SK & WANG JJ. 2016. Fundamental and molecular composition characteristics of biochars produced from sugarcane and rice crop residues and by-products. Chemosphere 142: 4-13.

KHADHRAOUI M, WATANABE T & KURODA M. 2002. The effect of the physical structure of a porous Ca-based sorbent on its phosphorus removal capacity. Water Res 36: 3711-3718.

KLOSS S, ZEHETNER F, DELLANTONIO A, HAMID R, OTTNER F, LIEDTKE V, SCHWANNINGER M, GERZABEK MH & SOJA G. 2012. Characterization of slow pyrolysis biochars: Effects of feedstocks and pyrolysis temperature on biochar properties. J Environ Qual 41: 990-1000.

KOSMULSKI M. 2001. Chemical Properties of Material Surfaces, Surfactant Science. CRC Press.

LI R, WANG JJ, ZHOU B, AWASTHI MK, ALI A, ZHANG Z, LAHORI AH & MAHAR A. 2016. Recovery of phosphate from aqueous solution by magnesium oxide decorated magnetic biochar and its potential as phosphate-based fertilizer substitute. Bioresour Technol 215: 209-214.

LIM SF, ZHENG YM & CHEN JP. 2009. Organic arsenic adsorption onto a magnetic sorbent. Langmuir 25: 4973-4978.

LIU P, LIU WJ, JIANG H, CHEN JJ, LI WW & YU HQ. 2012. Modification of bio-char derived from fast pyrolysis of biomass and its application in removal of tetracycline from aqueous solution. Bioresour Technol 121: 235-240.

LU C, LIU C & RAO GP. 2008. Comparisons of sorbent cost for the removal of Ni^{2+} from aqueous solution by carbon nanotubes and granular activated carbon. J Hazard Mater 151: 239-246.

MACHALA L, TUČEK J & ZBOŘIL R. 2011. Polymorphous transformations of nanometric iron(III) oxide: A review. Chem Mater 23: 3255-3272.

MAHER BA. 1988. Magnetic properties of some synthetic sub-micron magnetites. Geophys J Int 94: 83-96.

MAKRIS KC, HARRIS WG, O'CONNOR GA & EL-SHALL H. 2005. Long-term phosphorus effects on evolving physicochemical properties of iron and aluminum hydroxides. J Colloid Interface Sci 287: 552-560.

MOHAN D, KUMAR H, SARSWAT A, ALEXANDRE-FRANCO M & PITTMAN CU. 2014. Cadmium and lead remediation using magnetic oak wood and oak bark fast pyrolysis bio-chars. Chem Eng J 236: 513-528.

OH TK, CHOI B, SHINOGI Y & CHIKUSHI J. 2012. Effect of pH conditions on actual and apparent fluoride adsorption by biochar in aqueous phase. Water Air Soil Pollut 223: 3729-3738.

PARK H, AYALA P, DESHUSSES M, MULCHANDANI A, CHOI H & MYUNG N. 2008. Electrodeposition of maghemite (γ-Fe2O3) nanoparticles. Chem Eng J 139: 208-212.

RAJ A, RAJU K, VARGHESE HT, GRANADEIRO CM, NOGUEIRA HIS & YOHANNAN PANICKER C. 2009. IR, Raman and SERS spectra of 2-(methoxycarbonylmethylsulfanyl)-3,5-dinitrobenzene carboxylic acid. J Braz Chem Soc 20: 549-559.

SANTOS AFM, MACEDO LJA, CHAVES MH, ESPINOZA-CASTAÑEDA M, MERKOÇI A, LIMAC FDCA & CANTANHÊDE W. 2016. Hybrid self-assembled materials constituted by ferromagnetic nanoparticles and tannic acid: A theoretical and experimental investigation. J Braz Chem Soc 27: 727-734.

SHI Z, LIU F & YAO S. 2011. Adsorptive removal of phosphate from aqueous solutions using activated carbon loaded with Fe(III) oxide. New Carbon Mater. 26: 299-306.

SUN P, HUI C, AZIM KHAN R, DU J, ZHANG Q & ZHAO YH. 2015. Efficient removal of crystal violet using Fe_3O_4-coated

biochar: the role of the Fe3O4 nanoparticles and modeling study their adsorption behavior. Sci Rep 5: 12638.

TAN X, LIU Y, ZENG G, WANG X, HU X, GU Y & YANG Z. 2015. Application of biochar for the removal of pollutants from aqueous solutions. Chemosphere 125: 70-85.

TEJA AS & KOH PY. 2009. Synthesis, properties, and applications of magnetic iron oxide nanoparticles. Prog Cryst Growth Charact Mater 55: 22-45.

WANG SJ, ZHU WX, LIAO DW, NG, CF & AU, CT, 2004. In situ FTIR studies of NO reduction over carbon nanotubes (CNTs) and 1wt.% Pd/CNTs. Catal Today 93-95: 711-714.

XIANG H, LIU C, PAN R, HAN Y & CAO J. 2014. Magnetite for phosphorus removal in low concentration phosphorus-contained water body. Adv Environ Res 3: 163-172.

YAO Y, GAO B, CHEN J & YANG L. 2013. Engineered biochar reclaiming phosphate from aqueous solutions: Mechanisms and potential application as a slow-release fertilizer. Environ Sci Technol 47: 8700-8708.

YAO Y, GAO B, INYANG M, ZIMMERMAN AR, CAO X, PULLAMMANAPPALLIL P & YANG L. 2011. Removal of phosphate from aqueous solution by biochar derived from anaerobically digested sugar beet tailings. J Hazard Mater 190: 501-507.

ZHANG M & GAO B. 2013. Removal of arsenic, methylene blue, and phosphate by biochar/AlOOH nanocomposite. Chem Eng J.226: 286-292.

ZHANG M, GAO B, VARNOOSFADERANI S, HEBARD A, YAO Y & INYANG M. 2013. Preparation and characterization of a novel magnetic biochar for arsenic removal. Bioresour Technol 130: 457-462.

ZHANG M, GAO B, YAO Y, XUE Y & INYANG M. 2012. Synthesis of porous MgO-biochar nanocomposites for removal of phosphate and nitrate from aqueous solutions. Chem Eng J 210: 26-32.

ZHENG H, WANG Z, ZHAO J, HERBERT S & XING B. 2013. Sorption of antibiotic sulfamethoxazole varies with biochars produced at different temperatures. Environ Pollut 181: 60-67.

ZHONG ZY, XIONG ZT, SUN LF, LUO JZ, CHEN P, WU X, LIN J & TAN KL. 2002. Nanosized nickel(or cobalt)/graphite composites for hydrogen storage. J Phys Chem B 106: 9507-9513.

ZHOU YF & HAYNES RJ. 2010. Sorption of heavy metals by inorganic and organic components of solid wastes: Significance to use of wastes as low-cost adsorbents and immobilizing agents. Crit Rev Environ Sci Technol 40: 909-977.

TERESA CRISTINA F. SILVA[1]
https://orcid.org/0000-0002-1144-4665

LEONARDUS VERGÜTZ[2,3]
https://orcid.org/0000-0002-4457-8782

ANDERSON A. PACHECO[2]
https://orcid.org/0000-0002-2315-354X

LARISSA F. MELO[1]
https://orcid.org/0000-0001-6882-5875

NATALIA S. RENATO[2]
https://orcid.org/0000-0001-6168-8257

LEÔNIDAS C.A. MELO[4]
https://orcid.org/0000-0002-4034-4209

[1]State University of Minas Gerais at Ubá, Ave. Olegário Maciel, 1427, Industrial, 36500-000 Ubá, MG, Brazil

[2]Federal University of Viçosa, Ave. PH Rolfs, s/n, Campus da UFV, 36570-900 Viçosa, MG, Brazil

[3]Mohammed VI Polytechnic University, UM6P, 43150, Ben Guerir, Morocco

[4]Federal University of Lavras, Campus da UFLA, Aquenta Sol, 37200-000 Lavras, MG, Brazil

Correspondence to: **Natalia dos Santos Renato**
E-mail: natalia.renato@ufv.br

Author contributions

Teresa Cristina Fonseca Silva: Conceptualization, Methodology, Investigation, Writing - original draft, Writing - review & editing, Leonardus Vergütz: Conceptualization, Supervision, Writing - review & editing, Anderson Almeida Pacheco: Methodology, Writing - review & editing, Larissa de Freitas Melo: : Methodology, Writing - original draft, Natalia dos Santos Renato: Methodology, Writing - review & editing, Leônidas Carrijo Azevedo Melo: Methodology, Writing - review & editing.